HEDL-SA 1335

(25)

COMPUTER SIMULATION AND DAMAGE FUNCTION ANALYSIS*

D. G. Doran and R. L. Simons

Hanford Engineering Development Laboratory
Richland, Washington

*This paper is based on work performed by Hanford Engineering Development Laboratory, Richland, Washington, operated by Westinghouse Hanford Company, a subsidiary of Westinghouse Electric Corporation, under United States Energy Research & Development Administration Contract EY-76-C-14-2170.

COMPUTER SIMULATION AND DAMAGE FUNCTION ANALYSIS

D. G. Doran and R. L. Simons

I. INTRODUCTION

It is clear that neutron radiation damage to structural materials is a serious consideration in developing economical nuclear power. That such damage is generally sensitive to neutron energy is well known. Because the test spectra in which radiation effects data are obtained are generally different from the design spectra to which components are to be exposed, procedures are needed for taking spectrum differences into account in correlating and applying test data. The purpose of this paper is to describe such a procedure. It involves the combined use of two different types of computer calculations. One is "damage function analysis", in which the computer is used to solve interatively a set of integral equations in order to deduce the energy dependences of specific types of radiation damage. The other is the atomistic simulation by computer of defect production and annealing in a metal. Both these techniques are under active development, but the emphasis here is on their application. Brief descriptions will be given of both techniques and their application to the analysis of the energy dependence of the ductility of 20% cold-worked type 316 stainless steel.

II. COMPUTER SIMULATION OF DISPLACEMENT DAMAGE PRODUCTION

In any consideration of the correlation of radiation damage produced in different environments, an accurate description of the production of displacement damage is fundamental. Such a description provides 1) quantities for quantitative damage models, 2) concepts for conceptual models, and 3) parameters for the inevitable attempts at single parameter correlations.

The important quantities for correlation studies are the numbers, types, and configurations of the defects produced by a primary knockon atom (PKA) as a function of its energy. PKA energies of interest range from displacement threshold values of tens of eV to several MeV. The processes following the transfer of energy to a PKA may be viewed as taking place in three phases. The first phase extends from the creation of the primary to that time (10^{-14} - 10^{-13} sec) when the energy of the most energetic atom in the cascade falls below T_d, the threshold energy required to produce a permanent displacement in an otherwise undisturbed lattice. This is essentially the regime treated by cascade simulation codes such as MARLOWE and CASCADE.

There then follows a phase during which many lattice atoms surrounding displaced atoms are involved in numerous subthreshold encounters, resulting in a much disturbed, highly excited region of lattice. This second phase lasts from the end of cascade expansion until sufficient order is restored to distinguish distinct and stable vacancies, interstitials, and clusters throughout the cascade region. The significance of this phase stems from the fact that, except for the sum total of formation energies for the eventually stable vacancies, interstitials, and clusters, the energy deposited by the radiation is spent causing atom turbulence in the neighborhood of the cascade as the energy flows out to the rest of the lattice atoms. For this phase a period of 10^{-12} to 10^{-11} seconds is required during which local order is sufficiently re-established for diffusion processes to proceed once again by classical thermal activation. Current work is emphasizing this phase -- a dynamical simulation code such as COMENT is required.

Finally there is the third phase, the short-term annealing phase, characterized by activation processes. During this phase, the defects either annihilate, cluster, or escape from the cascade to be absorbed by other sinks. We have previously reported simulations of cascade production and annealing in fcc lattices. The first phase was obtained using the binary collision approximation as employed in either

the code CASCADE or version 10 of the code MARLOWE. In the current analysis, only results based on the latter were used because they covered the broadest energy range. The code uses a simple Kinchin-Pease displacement criterion in which any atom receiving an energy $\geq E_d$ is displaced. If the incident atom leaves a collision with energy $< E_d$, it is assumed to replace the displaced atom. For the computer runs used in this work, E_d was set at 25 eV.

Tables of defect coordinates served as direct input to a (third phase) random walk annealing code HAPFCC; i.e., no second phase description was attempted. Since MARLOWE does not determine the actual location of an interstitial, the first step was to assign each interstitial to a randomly chosen neighboring lattice site and to assign a randomly chosen <100> split interstitial orientation. In this pre-anneal stage, an annihilation region (AR) was imposed and clusters identified. The 32 site AR was based on the static variational calculations of Johnson; it is quite similar to the instability region found in the Brookhaven dynamical calculations using a different interatomic potential. The AR was treated as a square well -- certain annihilation within it and no influence on defect motion outside it. Cluster formation, on the other hand, was given a "softer" treatment in which defect jump probabilities were influenced by nearby like defects -- a shorter range of influence for vacancies than for interstitials. Defect behavior was based on Johnson's α-iron model in which the mobile species were mono-, di-, and tri-interstitials and mono-, di-, tri-, and tetra-vacancies.

The elevated temperature (nominally 500°C) anneal was carried out in the following stages of typically 1000 time steps each (approximate real time intervals at 500°C are indicated):

a. Interstitial migration with a spectrum of jump probabilities (real time $\sim 10^{-9}$ sec.). The uncorrelated jump probability of an I_1 was 0.5.

b. Vacancy migration with a spectrum of jump probabilities (real time $\sim 10^{-4}$sec.). The jump probability of the most mobile defect (V_2) was taken as unity. Mobile interstitials present at the beginning of this stage or created during the stage were moved (at time of creation) a predetermined number of steps or until their separation from all other defects exceeded a predetermined value.

c. Vacancy migration with all jump probabilities set to unity in order to permit significant monovacancy migration (real time $\sim 10^{-2}$sec.). At the end of this stage all mobile defects were assumed to have escaped from the cascade and were subsequently ignored. No dissociation of clusters was permitted. Ten cascades having randomly selected knockon directions were processed at each energy in the range 0.5 to 100 keV.

The effects of annealing on the spatial distribution of defects is illustrated in Figures 1 and 2. Two projections are given of the three-dimensional configurations of typical Beeler 5 and 20 keV cascades. The take-off point (200, 200, 200) and direction of the PKA are indicated by X's and squares, respectively, and cluster sizes are included in the post-anneal plots. Any mobile interstitials remaining in the field of view have been deleted.

The results of these simulations can be expressed as defect production functions of the primary knockon atom energy T. For example, the number of residual defect pairs surviving short term annealing is given by

$$N_{pair} = 5.00\ T^{0.80} - 0.38 \qquad 0.50 \leq T \leq 100 \text{ keV} \qquad (1a)$$

$$= 4.6\ T + 0.2 \qquad 0.04 \leq T < 0.5 \text{ keV} \qquad (1b)$$

The residual number of mobile vacancies, that is, the number escaping from the

cascade, can be described by

$$N_{vac} = 0.52\,(T^2 + 42T)^{1/2} \qquad 0.50 \leq T \leq 100 \text{ keV} \qquad (2a)$$

$$= 4.6\,T + 0.2\ . \qquad 0.04 \leq T < 0.50 \text{ keV} \qquad (2b)$$

The defect functions were extrapolated above 100 keV by assuming linearity with the damage energy (Lindhard model) and matching value and slope at 100 keV. The data in the 20 to 100 keV range are reasonably consistent with this assumption. Note that the production of immobile vacancy clusters is negligible below 0.5 keV so that the same function is used for extrapolation to lower energies in each case.

The defect functions have been combined with primary recoil spectra due to monoenergetic neutrons to produce neutron defect production cross sections. The mobile vacancy cross section is compared with the displacement cross section in Figure 1.

III. DAMAGE FUNCTION ANALYSIS

In much of the literature, the term "damage function" is used for any energy dependent damage cross section. For example, the cross section may describe energy deposition, displacement production, cluster production, etc. Therefore, we shall use the term "effective damage function" (EDF) to mean a semi-empirically derived function of energy that expresses the effective energy dependence of a particular property change of a particular material at a particular irradiation temperature. The EDF is concerned only with a particular damage level that results from neutron irradiation. It conveys no information about the fluence dependence of intermediate stages of damage. The basic assumption is that the fluence required to reach a particular property level (at a given irradiation temperature) depends only on the spectrum. We can express this mathematically as follows. Let P denote the particular property level of interest (e.g., 5% total elongation); $G_p(E)$, the EDF

associated with P; $\phi_j(E)$, a neutron spectrum normalized to unit flux; and $(\phi t)_{Pj}$, the fluence required in the j^{th} test spectrum to produce P. Then

$$P = (\phi t)_{Pj} \int_0^\infty G_p(E)\, \phi_j(E) dE \qquad j=1,\ldots,N\ , \qquad (3)$$

Since $\phi_j(E)$ is normalized to unit flux, the right side of Eq. (3) is just the spectrum averaged value of $G_p(E)$ in the j^{th} spectrum and we can write

$$\frac{P}{(\phi t)_{Pj}} = \bar{G}_{Pj} \qquad j=1,\ldots,N\ . \qquad (4)$$

The N values of the left side of Eq. (4) are the experimental data from which $G_p(E)$ must be deduced by solving N Eqs. (3).

An iterative solution procedure is used at HEDL, employing the computer code SAND-II to solve for $G_p(E)$. The procedure is as follows. Having obtained the necessary $\phi_{Pj}(E)$ and $\bar{G}_{Pj} = P/(\phi t)_{Pj}$, the solution begins with an assumed energy dependence $G_p^\circ(E)$. $G_p^\circ(E)$ should contain the available information on the damage mechanism(s) associated with the particular property change of concern. It might represent the variation with energy (absolute magnitude is not important) of the displacement cross section, a residual defect cross section, a cluster cross section, a transmutation cross section, etc. The computer code SAND-II calculates the property change expected in the different spectra according to $G_p^\circ(E)$, determines the differences between calculated and experimental values, and then modifies $G_p^\circ(E)$ iteratively to reduce the differences to within acceptable experimental uncertainties.

If the data have been obtained in spectra covering the complete energy range of interest, then the final EDF solution can be reasonably unique; that is, it can be essentially independent of the starting function. The differences between starting

and derived functions can therefore provide clues to the active damage mechanism(s), depending on uncertainties and solution uniqueness. Generally, however, there are neutron energy regions for which no data are available; the fewer the data, the more the result depends on the starting function assumed. In the extreme case of a property change measured in only one spectrum, that data point serves to normalize the input damage function and the energy dependence is based wholly on theory.

Three factors are considered explicitly in determining the uncertainty in $G_p(E)$: (1) errors related to the material property measurement, (2) errors in the flux-fluence spectra, and (3) mathematical nonuniqueness of the solution.

A critical and time consuming part of the analysis is the determination of the spectrum and fluence to be associated with each data point. Since the property change measurements are seldom at the designated level P, it is usually necessary to interpolate or extrapolate the data obtained in a specific spectrum to the level P by assuming a fluence dependence. If sufficient data are obtained in one spectrum to define the fluence dependence, the same dependence may be assumed to hold in any other spectrum. Another approach is to try to represent the exposure dependence of all the data with a function of an energy dependent damage parameter. This "analytical correlation model" can then be used for interpolation or extrapolation of data in order to determine the appropriate fluence, $(\Phi t)_{Pj}$, for each of the N spectra. Clearly, if the correlation model fits the data well, the unfolded EDF should have the same energy dependence as the damage parameter used in the model over the spectral range of the data. [The damage parameter, appropriately normalized, would serve as $G^{\circ}(E)$.] If, furthermore, some physical significance can be attributed to the damage parameter, it may provide a basis for extrapolating beyond the spectral range of the data. The development of physically significant damage parameters is a prime objective of the computer simulation studies of damage production described earlier. An example of such a correlation analysis will now be given.

IV. CORRELATION ANALYSIS FOR TOTAL ELONGATION OF 316 SS

The primary data set was tensile test data (specifically total elongation) for 20% cold-worked type 316 stainless steel irradiated in EBR-II. The data were obtained in Rows 2 and 4 over a vertical traverse corresponding to a mean neutron energy range of 0.27 to 0.83 MeV, about the maximum energy spread possible in EBR-II. At a given vertical distance above or below midplane, the spectra at Rows 2 and 4 are nearly the same. Since the total fluences for the Row 2 data (maximum of 7×10^{22} n/cm^2-s) were about double those for Row 4, this data set provided an opportunity to separate fluence and spectrum effects (see Figure 4). The irradiation temperatures were 370-420°C and the test temperatures were 370°C or 425°C. Some data from the Oak Ridge High Flux Isotope Reactor (HFIR) were also available. The combined set of data (12 points) represents a fluence and spectrum range that is about the best that can be currently obtained in fission reactors.

The form of the correlation model was

$$P = P_o - P_s [1 - \exp (- \beta \bar{f} \phi t)]$$

where P_o, P_s and β are adjustable constants determined by a nonlinear least squares analysis. The total fluence is indicated by ϕt and a spectrum-averaged damage parameter by $\bar{f}$. A number of physically significant damage parameters f(E) were examined, covering a wide range of energy dependences. Damage parameters obtained from computer simulation include the number of interstitial clusters, the number of residual interstitial-vacancy pairs, and the number of mobile vacancies. Other parameters tested were 1) the number of cascades, 2) the number of displaced atoms, 3) the mean neutron energy, and 4) the total fluence. The last two represent the extremes in high and low energy dependences, respectively.

A sample of the data used in this analysis is shown in Table 1, and the fitted parameters are given in Table 2. Table 2 includes also the sum of the residuals resulting from a nonlinear least squares analysis. The best fit was obtained with the mobile vacancy cross section MV(E). The quality of the fit is graphically illustrated in Figure 5.

The complete damage function analysis is not yet finished. While the energy dependence of the EDF will certainly be that of MV(E), the analysis provides a systematic means of introducing uncertainties for the purpose of estimating an upper bound EDF.

V. DISCUSSION

The primary purpose of this paper has been to illustrate a damage correlation methodology that incorporates theoretical analyses of radiation damage with engineering property change data. The connection between the production of mobile vacancies and the change in total elongation is tenuous. One should not attach too much physical significance to MV(E) per se because current research with better simulation codes and improved experiments on defect production may result in significant changes. However, the reduced energy dependence relative to the displacement cross section is significant, because the displacement cross section is most often used to project data to spectra much different from those in which they were obtained.

TABLE 1

EXAMPLE OF EXPERIMENTAL DATA AND CORRESPONDING VALUES OF SEVERAL DAMAGE PARAMETERS

SPECTRUM EBR-II R (cm)	Z (cm)	TOTAL ELONGATION %	IRRAD. TEMP. (°C)	TOTAL FLUENCE (10^{22}n/cm^2-s)	$\bar{E}\cdot$ TOTAL FLUENCE (10^{22}MeV/cm^2-s)	DISPLACEMENTS PER ATOM	RESIDUAL PAIRS PER ATOM	MOBILE VACANCIES PER ATOM	INTERSTITIAL CLUSTERS PER ATOM	CASCADE PER ATO
4.2	-6.4	2.0	380	7.02	5.84	30.3	11.2	3.91	0.302	0.266
7.9	-6.4	4.8	380	3.28	2.75	14.2	5.22	1.83	0.141	0.124
4.2	44.5	11.5	420	1.65	0.455	3.15	1.29	0.533	0.0274	0.074
7.9	44.7	16.8	420	0.770	0.212	1.47	0.601	0.289	0.0128	0.034

TABLE 2

VALUES OF ADJUSTABLE CONSTANTS IN DAMAGE CORRELATION MODEL CORRESPONDING TO SEVERAL DAMAGE PARAMETERS

$$P = P_o - P_s [1 - \exp(-\beta \cdot \bar{f} \cdot \phi t)]$$

Parameter / Constant	Total Fluence	Mean Energy $\bar{E}$	Displacements	Residual Pairs	Mobile Vacancies	Interstitial Clusters	Cascades
P_o	27.1	20.5	21.2	21.7	22.7	20.6	28.5
P_s	24.8	17.6	18.5	19.1	20.2	17.7	26.2
β	68.5	130.	0.207	0.539	1.44	22.1	17.0
Sum of Squares of Residuals Relative to Mobile Vacancies	2.92	2.59	1.84	1.46	1.00	2.48	5.80

FIGURE CAPTIONS

1. A two-dimensional projection of a displacement cascade produced by a 5 keV atom displaced from 200, 200, 200 in the direction shown by the arrow. Vacancies and interstitials are indicated by squares and X's, respectively. Distances are expressed in half-lattice units (~1.8 Å). Both pre-anneal and post-anneal configurations are shown.

2. A compact 20 keV cascade. See caption for Figure 1.

3. Comparison of the energy dependence of a theoretical displacement cross section for stainless steel and a mobile vacancy cross section derived by computer simulation.

4. Total elongation of 20% CW 316 SS as function of total fluence. Dashed lines connect points corresponding to the same neutron spectrum (same letter designation).

5. Total elongation of 20% CW 316 SS as function of mobile vacancies per atom.

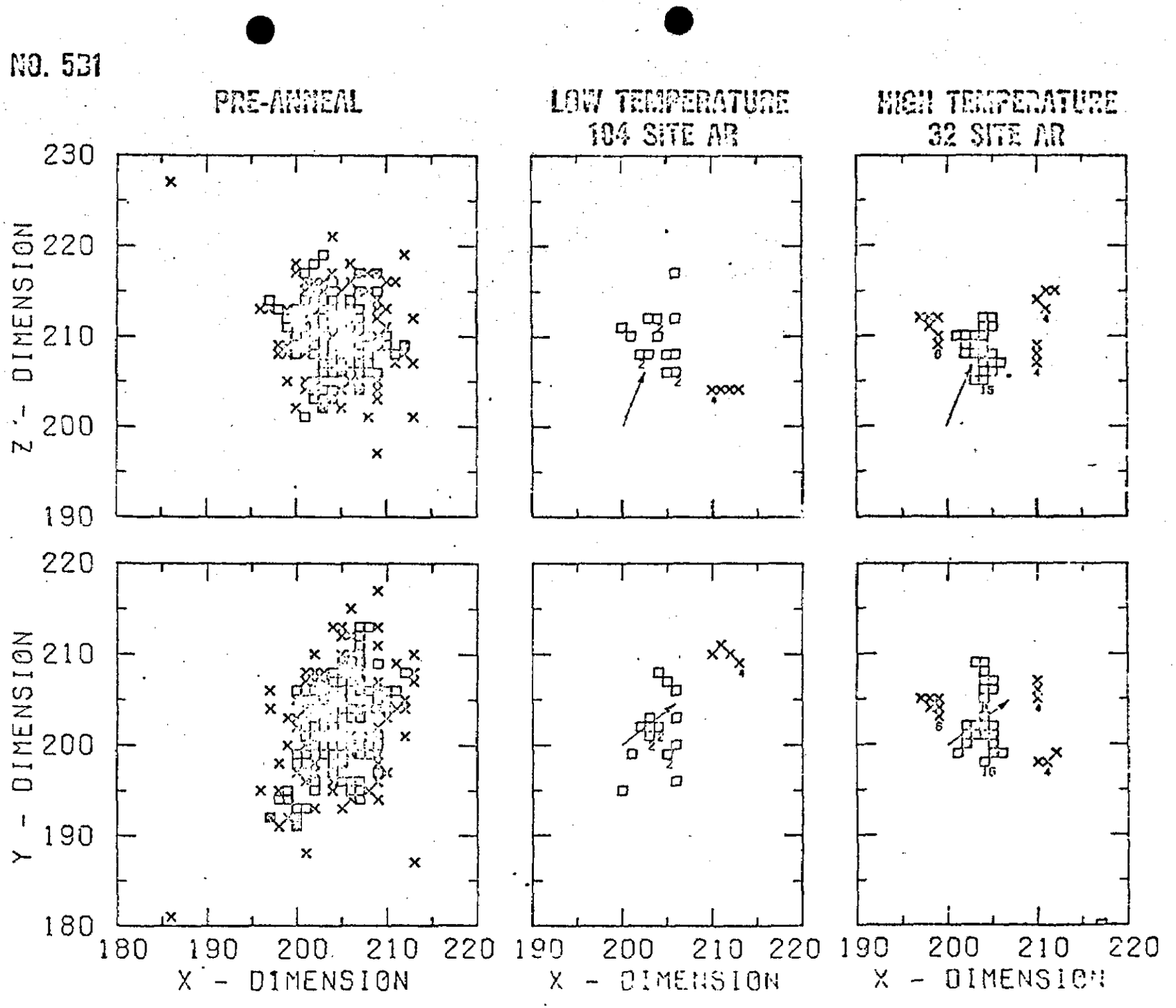

Figure 1

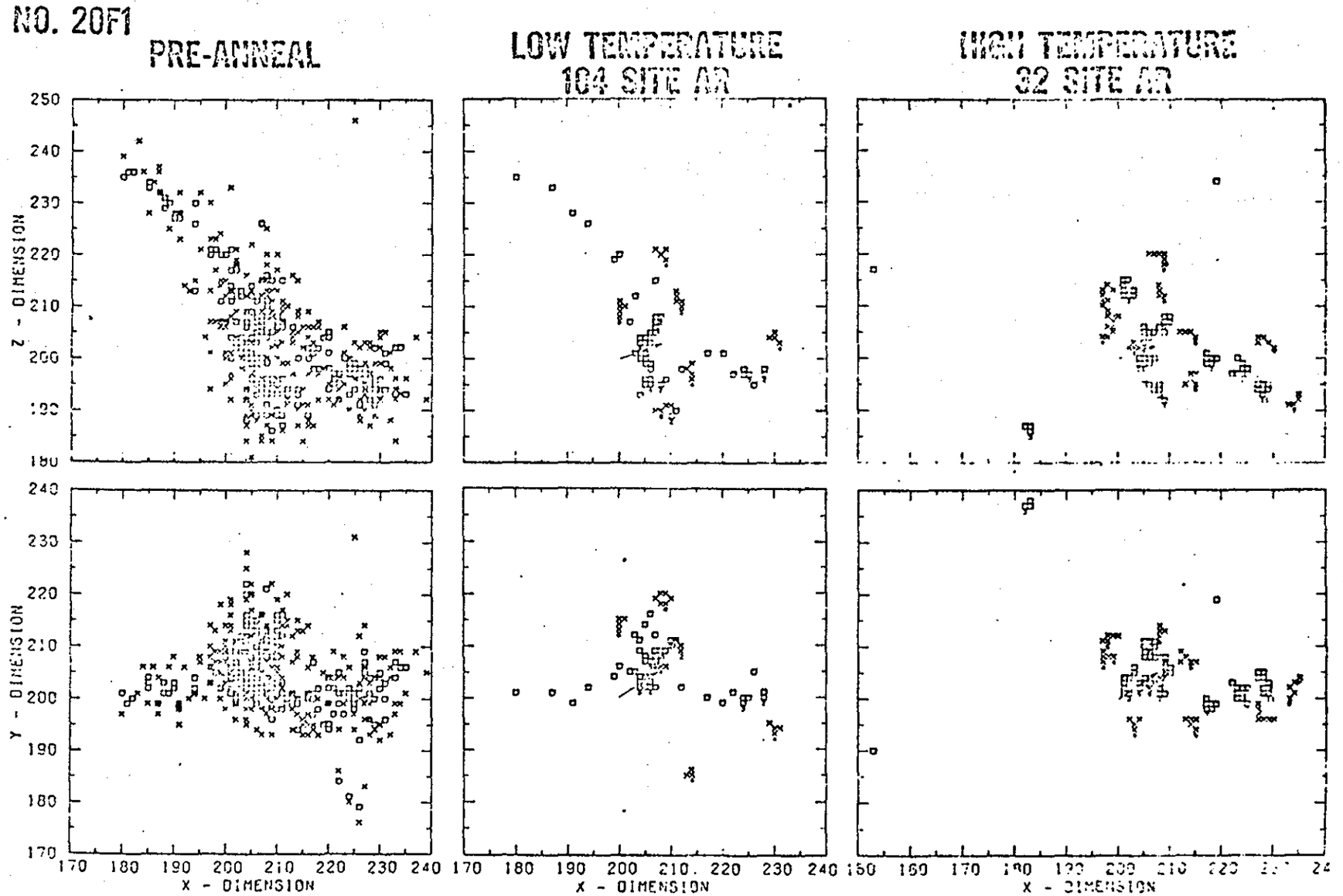

Figure 2

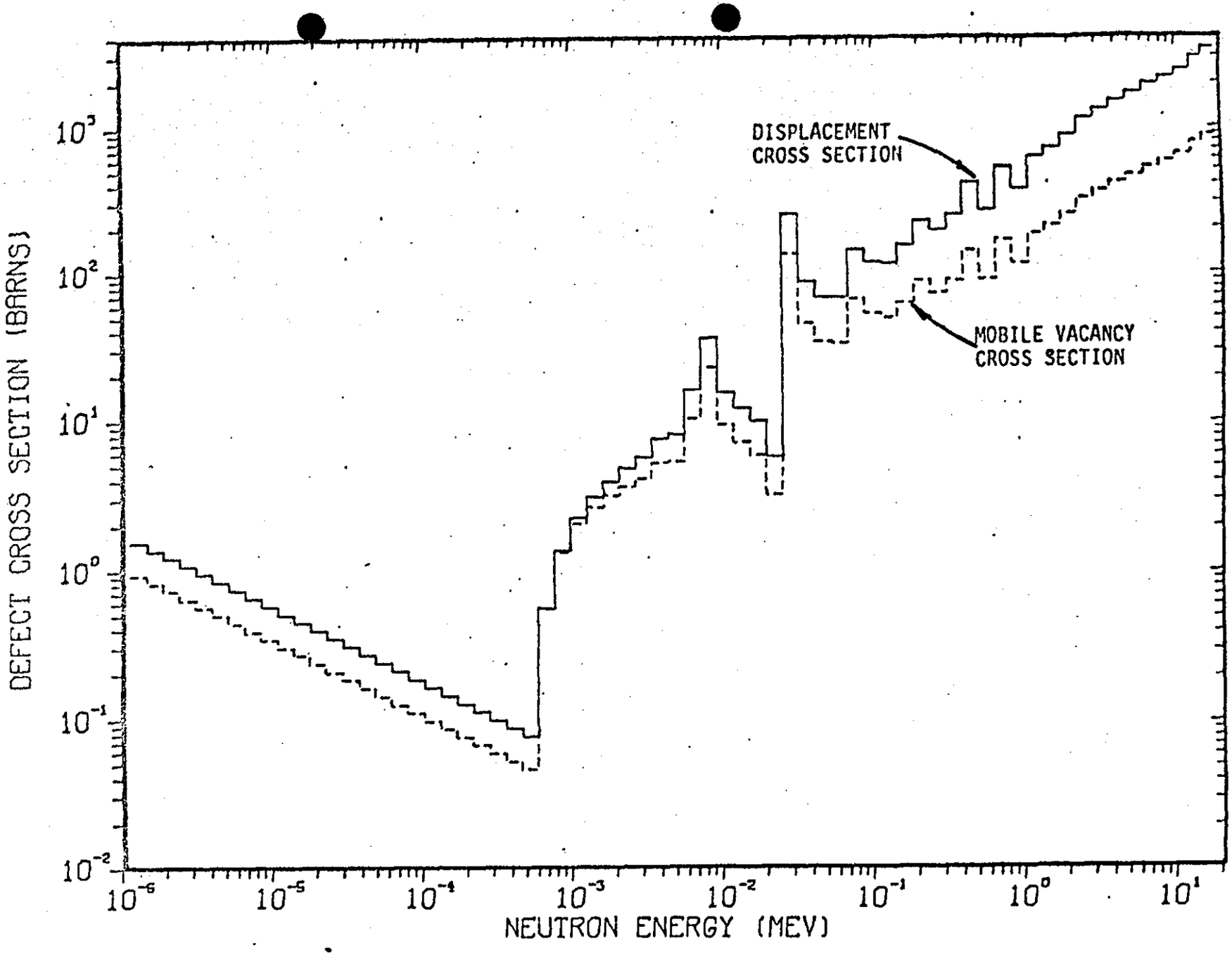

FIGURE 3 COMPARISON OF THE ENERGY DEPENDENCE OF A THEORETICAL DISPLACEMENT CROSS SECTION FOR STAINLESS STEEL AND A MOBILE VACANCY CROSS SECTION DERIVED BY COMPUTER SIMULATION.

FIGURE 4

SEMI-LOGARITHMIC 46 5490
3 CYCLES X 70 DIVISIONS MADE IN U.S.A.
KEUFFEL & ESSER CO.

10/25/77